CORE
Metadata, citation and similar papers at core.ac.uk
Provided by University of Malaya Students Repository

Chapter 3

Experimental

And

Analytical Techniques

3.1 Introduction

Lately, hydrogenated silicon (Si:H) thin films have been deposited using various techniques. Among them, the plasma enhanced chemical vapour deposition (PECVD) is the most favourable technique for depositing Si:H thin films. Optimization of the deposition conditions has resulted in the device quality of Si:H to become the motivation of most research on these materials. In this work, Si:H thin films were deposited by layer-by-layer (LBL) deposition technique using a home-built rf (13.56 MHz) PECVD system in the Low Dimensional Materials Research Centre, Department of Physics, University of Malaya. This chapter describes the two major parts of experimental and analytical techniques used on the Si:H films studied. The first part of this chapter describes the deposition system and the sample preparation procedures. This is followed by the description of the substrate cleaning procedures. The second part of this chapter presents the analytical instruments utilized in characterizing the films, and the characterization procedures and calculation techniques used to analyze the results obtained from the measurements. These characterization techniques include optical transmission spectroscopy, Fourier transform infrared (FTIR) spectroscopy, X-Ray Diffraction (XRD), Micro-Raman scattering spectroscopy, Micro-Photoluminescence spectroscopy, field emission electron microscope (FESEM) and high resolution transmission electron microscope (HRTEM). Figure 3.1 presents the flowchart of the methodology that involved in carrying out this work.

3.2 Deposition Technique

3.2.1 Plasma Enhanced Chemical Vapour Deposition (PECVD) System

The system used in the deposition of Si:H thin films in this work is a home built vertical configuration rf-PECVD system. This system, which was modified from a horizontal configuration direct current (d.c.) PECVD system in the laboratory, had been

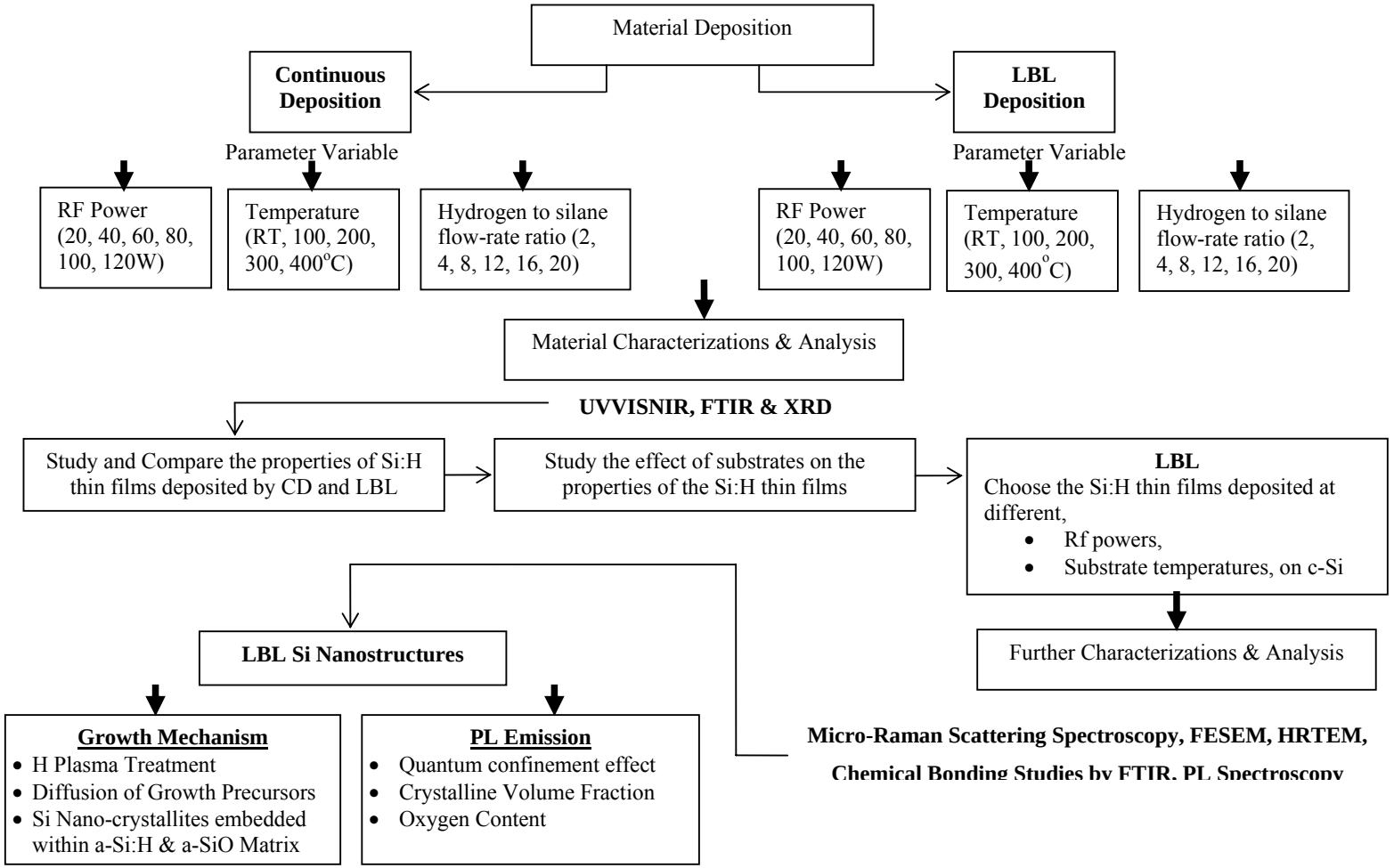

Figure 3.1: Flowchart of research methodology involved in this work.

used in the production of high quality hydrogenated amorphous silicon thin films by earlier researchers (Goh *et al.*, 2002; Lim *et al.*, 2004; Goh *et al.*, 2004, Goh *et al.*, 2006; Shi *et al.*, 2006; Shi *et al.*, 2007; Goh *et al.*, 2007). Basically, this system consists of five major components, which are the reaction chamber, the vacuum pumping system, the gases supply and distribution system, the electrical power supply system and the detoxification system. The schematic diagram of the rf-PECVD system is shown in Figure 3.2.

The cross-sectional view of the home-built reaction chamber is shown in Figure 3.3. The reaction chamber is made of stainless steel (SS) because it is resistant to corrosive gases, especially silane (SiH_4) gas, and does not react with the reacting gases. The dimensions of the reaction chamber are 300 mm in height, 150 mm in diameter and 6 mm in wall thickness. This design is able to achieve a high vacuum level of 4.0×10^{-5} mbar with the pumping of the diffusion pump. The top plate is connected with a SS rotary shaft feedthrough with ¼" SS tubing as a gas inlet. The feedthrough is used to support a shower head electrode, insulator and rf power contact with the electrode. The centre of the bottom plate is connected with a NW40 SS flexible host to baffle for further connection to the roughing pump (rotary vane pump 1) and diffusion pump. Also, this plate is used to connect to the electrical feedthrough, such as ground electrode contact, thermocouple and heater. Besides, this plate is also attached with NW16 connectors for vacuum gauges as pirani and penning gauges. The sample holder is in contact, on the bottom plate, with insulators and the ground electrode, the thermocouple and heater are attached to the sample holder as shown in Figure 3.3. As can be seen from the figure, the ground electrode is connected to the top of the substrate holder. The cartridge heater is inserted into the substrate holder. The top and bottom electrodes are electrically isolated from the body of the reaction chamber by Teflon insulators. The distance between the electrode and area of the electrodes are fixed at 5 cm 28 cm^2

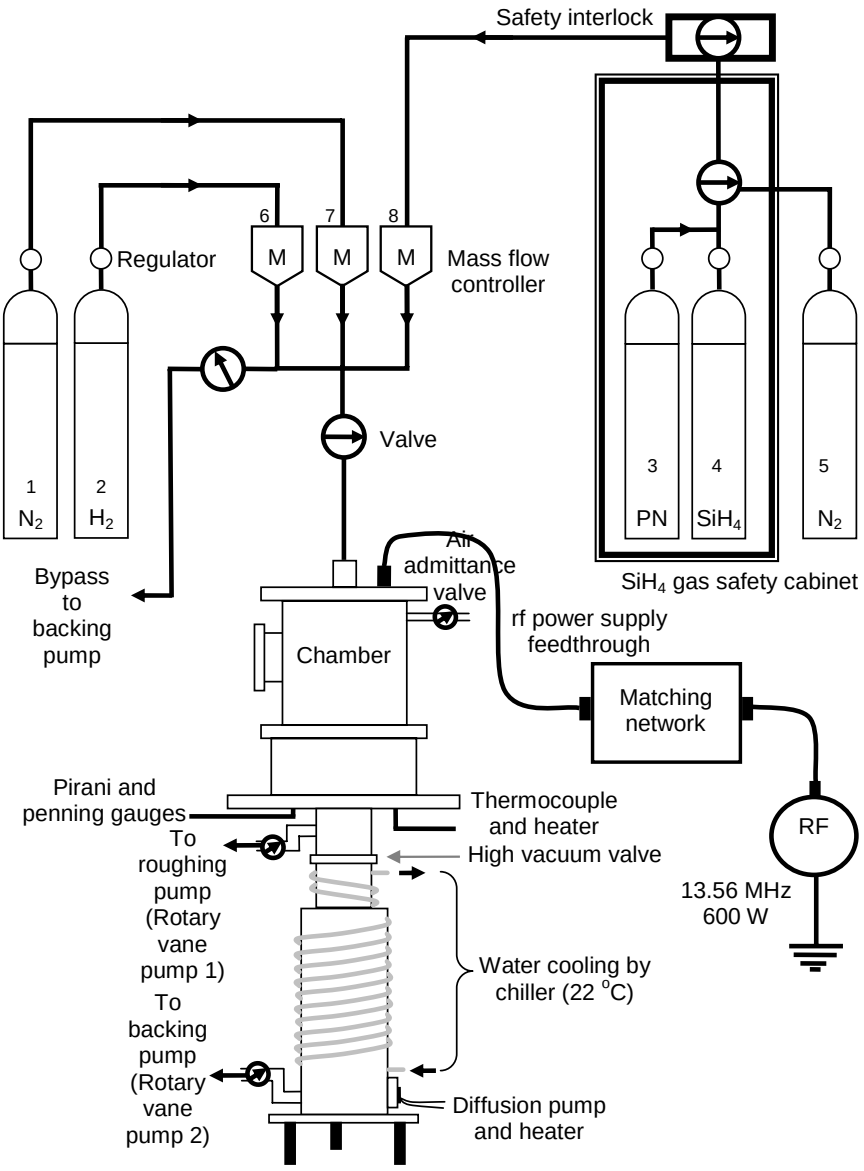

Figure 3.2: The schematic diagram of the PECVD system including the reaction chamber, the vacuum pumping system, the gases supply and distribution system, electrical power supply system and the gas detoxification system.

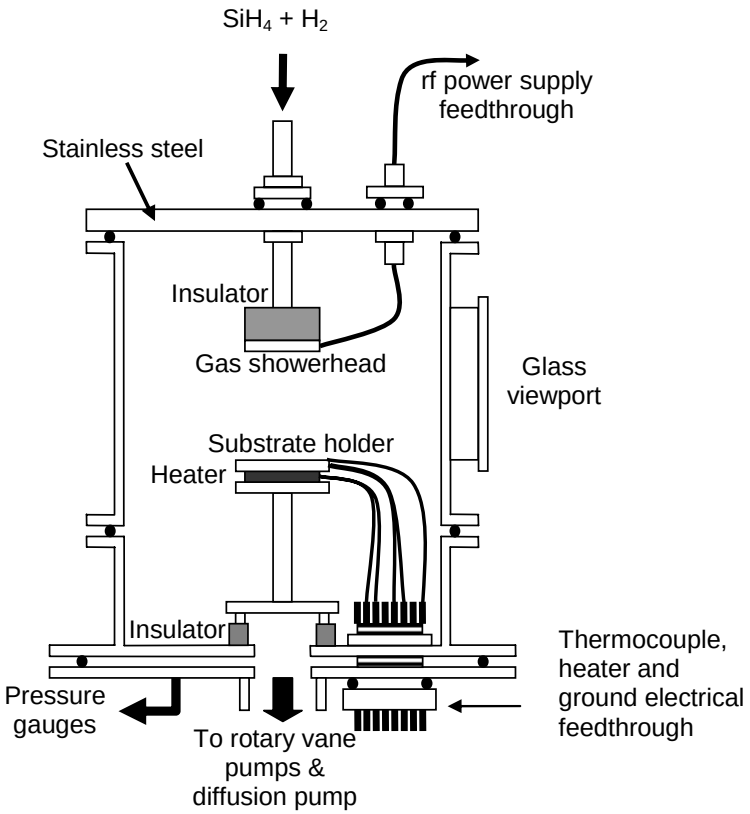

Figure 3.3: The schematic diagram of the reaction chamber for Si:H thin films.

respectively. The top of the substrate holder consists of four grooves (dimension of 2 cm × 2 ½ cm) with a depth of ½ cm for holding the substrates. Furthermore, these substrates are clamped with an aluminium plate as a mask. The thermocouple is fixed into the substrate holder and the head of the thermocouple is in contact with the glass substrate to measure the substrate temperature during the deposition.

For the pumping system, a rotary vane pump (model Edward E2M28) is used to evacuate the reaction chamber and to maintain the required pressure during the deposition process. This rotary vane pump is able to evacuate the reaction chamber to a vacuum level of 2.0×10^{-3} mbar. For a high vacuum level, the reaction chamber is pumped down until a vacuum level of 4.0×10^{-5} mbar by diffusion pump (model Edward F403 with heating power of 500 W). The pressures in the reaction chamber for low and high level vacuum are measured using pirani (Leybold vacuum gauge with model TTR91) and penning (Leybold vacuum gauge with model PTR 225) gauges, respectively, which are attached directly to the bottom plate of the reaction chamber through SS vacuum connectors.

To ensure that there is no sudden disruption in the power supply, the rotary vane pump is connected to a 10 kVA Uninterruptible Power Supply (UPS). This UPS can sustain the power supply for about 2 hours in case there is any interruption in the power supply. This is to ensure that silane gas is always in pumping and vacuum conditions.

The nitrogen gas is used to purge the gas line and reaction chamber before and after deposition to remove any contaminants in the gas lines and deposition system. Also, the nitrogen gas is directed into the rotary vane pump oil compartment to prevent the silane gas from condensing in the pump during deposition and also to dilute the gas before exiting through the exhaust lines. The excess silane gas exits via the exhaust line into the detoxification system, which is located outside of the laboratory.

In the gas distribution system, the four gases used in this work are silane, SiH_4 (99.9995 %), purified hydrogen, H_2 (99.999 %), purified nitrogen, PN (99.999 %) and industrial nitrogen, N_2 (99.9 %). The SiH_4 is used as a source gas for Si:H thin films deposition, and H_2 as a diluent gas, while PN and N_2 are used for purging the PECVD system, which includes the gas line, reaction chamber and roughing, before and after deposition. All these gases are distributed from the gas tanks inside the gas room to the reaction chamber via a gas distribution system. The gases are delivered through ¼" SS tubing using Swagelock connectors and valves to a gas distribution panel.

The SiH_4 gas tank is stored in the safety cabinet attached to an exhaust system, which is able to remove any SiH_4 gas in case of leakage. The SiH_4 gas tank has a special gas regulator, model AP1510S, which is connected to a special purging system. This purging system is connected to a N_2 gas cylinder. This special gas regulator has a pneumatic valve, which allows gas flow through it only when the pressure of N_2 is about 50 psi. This N_2 gas is connected to the regulator through a safety system. This safety system is particularly used for SiH_4 gas to stop the gas from flowing into the reaction chamber instantly in the case of emergency.

From the gas distribution panel, the gases enter the reaction chamber through the mass flow controller (MFC) with model of (Aalborg, GFC17), to monitor the gas flow-rate. Before the MFC, the gas pressure is controlled by metering valve (Swagelock, SS-4MG) to prevent high pressure of gas entering into the MFC. This is used to protect the valve inside the MFC from damage due to high pressure of gas flowing. On exiting the MFC, the gases pass through check valves (Swagelock, SS-CHS4-1/3), which are used to prevent back flow of the gases. The gases (SiH_4 and H_2) are mixed prior to entering the reaction chamber.

As shown in Figure 3.2, the bypass line is made for safety purposes, which allow the SiH_4 gas to be pumped out via the rotary pump directly if any blockage occurs

at the entrance of the MFC. Also, it is used to remove excess SiH_4 and other gases at a faster rate after the deposition process.

Finally, the excess of SiH_4 is transferred to a detoxification tank since SiH_4 gas is a highly toxic gas and is flammable when exposed to air. The detoxification tank will convert excess SiH_4 gas to a non-toxic form after the deposition process. Normally, N_2 gas is used to dilute the excess SiH_4 gas from the reaction chamber in the rotary and transfer it into the detoxification tank. The detoxification tank is a hard polymer tank and contains a solution of sodium permanganate ($KMnO_4$, M=158.04 g/mol). The outlet of the pump exhaust is connected to the tank by the exhaust pipe and it must be dipped into the bottom of the tank. This is to ensure that the chemical reaction of the SiH_4 gas and $KMnO_4$ is completed before the gas is exposed to the air. The residual SiH_4 gas in the reaction chamber is pumped out by the rotary pump into the tank through an exhaust line. The chemical reaction for neutralizing the residual SiH_4 gas is as given below (Tan, 1997),

$$8KMnO_4 + 3SiH_4 \rightarrow 8MnO_2 + 3SiO_2 + 8KOH + 2H_2O, \qquad (3.1)$$

The solution is changed every time its colour changes.

The electrical power supplies are divided into two main supplies including the plasma generating supplied by rf of 13.56 MHz power supply (ENI, 600 W) and the substrate heating supplied by voltage regulator (IBC Regavolt, 0-240 V A.C., 1 KVA). These electrical circuitries are installed in a power supply cabinet and are monitored by the electrical control panels on the display panel of the cabinet. The regavolt is used to supply the 240V A.C. power supply to the heater and temperature controller. The voltage supplied to the heater (Watlow firerod cartridge heater, 400 W) by regavolt is controlled by a temperature controller (Taishio TS501) to produce the required temperature and the temperature is measured by a chromel-alumel k-type thermocouple (measured temperature from room temperature to 500°C).

3.2.2 The Substrate Cleaning Procedure

In this work, the substrates used to deposit the Si:H thin films are p-type crystal silicon (c-Si) wafer and Corning glass. The cleaning process is very important to ensure that the cleanliness level is always high and also to remove contaminants on the substrate which may affect the properties of the film deposited on the substrate. The choice of cleaning techniques depends on the nature of the substrate, the type of contaminants and the degree of cleanliness required. Residues from manufacturing and packaging, lint, fingerprints, oil and airborne particulate matter are examples of frequently encountered contaminants.

Suitable reagents for substrate cleaning include aqueous solutions of acids and alkalis as well as organic solvents such as alcohols, ketones and chlorinated hydrocarbons. The cleaning effect of acids is due to the conversion of oxides and grease into water-soluble compounds. Alkaline agents dissolve fatty materials by saponification, which renders them wettable.

In ultrasonic cleaning, dissolution of residues is enhanced by the intense local stirring action of the shock wave created in the solvent. Thus, solvent saturated with impurities is continually carried away from the substrate surface and fresh, less saturated liquid is admitted. Mechanical vibrations induced in the substrate further aid loosening gross contaminants, such as particulate matter flakes.

Cleaning the substrate in a detergent solution cleans and removes surface contamination. Cleaning in detergent solution, however, is less effective than either of the other techniques. Rinsing in deionized water cleans and removes surface contamination produced during the cutting process. The drying process of substrates is also critical because recontamination can occur. Drying may be accomplished in a vapour degreaser, a clean oven, or with hot filtered air or nitrogen.

The effective cleaning of substrates has a strong effect on the adhesion properties of deposited films. Dust, inorganic and organic particles on the substrates should be cleaned off using a standard cleaning procedure. The glass substrates are ultrasonically cleaned in a beaker containing soap solution (Decon 90 with distilled water) to remove oil and gross dirt. Then the whole beaker is immersed into an ultrasonic bath for 15 minutes at a temperature of 60°C. The substrates are then rinsed in distilled water. To remove any oil deposits, the substrates are further rinsed in acetone (99.5 %, 58.08 g/mol) and finally in ethanol (95 %, 46.07 g/mol). After the cleaning process, the substrates are dried by industrial nitrogen gas (99.9 %) to prevent formation of water spots. Then, the cleaned substrates are immediately put into the reaction chamber and continue with the evacuation to the vacuum level. This procedure aims to prevent oxidation on the surface of the substrates. The cleaned substrates used as a background for characterizations usages are stored in a dry cabinet with humidity of 32 for maintaining the substrates' cleanliness and prevent contamination.

The cleaning process for the c-Si substrates begins with rinsing the substrates in deionized water and then the substrates are immersed in a beaker containing H_2O:HCl:H_2O_2 = 86:11:3 [HCl (37 %, 36.46 g/mol) and H_2O_2 (30 %, 34.01 g/mol)] solution for 5 minutes. Then, the substrates are rinsed again in deionized water. The next step is to immerse the substrates in a solution of H_2O:H_2O_2:NH_4OH: = 4:1:1 [NH_4OH (25 %, 17.03 g/mol)] for 5 minutes also followed by rinsing in deionized water. Finally, the substrates are immersed in a solution of H_2O: HF = 10:1 [HF (48 %, 20.01 g/mol)] for 5 minutes and followed by a final rinse in deionized water. This step is used to etch away surface oxide (native oxides or SiO_2) on the substrates (Goh, 2005). The cleaned c-Si substrates are dried using a nitrogen air gun and placed in the reaction chamber which is immediately evacuated. The vacuum in the reaction chamber will

ensure minimum oxide formation on the c-Si substrates. The methods used for substrate cleaning (c-Si and glass substrates) are referred to (Kern and Vossen, 1978; Kern, 1993).

3.2.3 Preparation Procedures for Hydrogenated Silicon (Si:H) Thin Films Using Continuous Deposition (CD) and Layer-by Layer (LBL) Deposition Techniques

The proper operation of the PECVD system for deposition of Si:H thin film is very important to ensure a successful and safe deposition process. The setup of the PECVD system has already been presented in Section 3.2.1. SiH_4, which is used in the deposition of Si:H thin films, is a toxic gas that reacts explosively with both air and water vapour. Therefore, it is essential to make sure that the system is free of any leakage. Contamination of the Si:H thin film produced can also be avoided if the system is leakage free. The post deposition procedure is just as important as the pre-deposition and deposition procedures during the deposition process. Removal of excess SiH_4 after a deposition process is a very important process. Excess SiH_4 in the gas lines forms solid residue in the system in the form of powder, especially at the points where the gas flow has to slowdown, particularly at the needle valve, mass flowcontroller and joint connections. This effect can block gas lines and result in high pressures at these points, which can be very dangerous, especially when SiH_4 gas is concerned.

The reaction chamber must be cleaned after every deposition process to remove deposits left from the previous deposition. A wet sand paper is used to remove the coated film and other contaminants on all the metal surfaces. Then the metal surface is cleaned throughly again using acetone to remove the water and oil contaminants. The cleaned substrates are then placed in the cleaned reaction chamber. The two ends of the reaction chamber are closed with two flat stainless steel plates (refer to Figure 3.3) and sealed properly with greased Viton O-rings. The system is then set-up for deposition.

The pumping process of the reaction chamber is divided into two stages as stated in Section 3.2.1. Backing and roughing pumping to about 2.0×10^{-3} mbar is done by rotary pumps and continue by diffusion pump to achieve 4.0×10^{-5} mbar at high vacuum level. Before switching on the rotary vane pump, all the valves within the system (refer to Figure 3.2) (roughing valve and air admittance valve) are closed tightly. The rotary vane pump 1 as a roughing pump is then switched ON to evacuate the vacuum line below the roughing valve. The roughing valve is then opened and the reaction chamber is evacuated to a pressure of 2.0×10^{-3} mbar. The gas lines to the system are then opened stage by stage from the reaction chamber to the gas cylinder. When the pressure is back to 2.0×10^{-3} mbar with the gas lines fully opened, all the valves from gas lines to the reaction chamber are closed. The diffusion pump and rotary vane pump 2 as a backing pump are switched ON to evacuate the line of the diffusion pump as shown in Figure 3.2. The roughing valve is closed and the high vacuum valve (Figure 3.2) is opened after 30 minutes for the diffusion pump to achieve a high pumping rate. During the diffusion pumping process, the chiller is switched ON and supplies a water flow with a temperature of 22°C to circulate the outer body of the diffusion pump (Figure 3.2) by ¼ inch SS tubing (Swagelok, SS-T4-S-035-6ME). The purpose of the cooling is to enhance pumping efficiency of the diffusion pump in order to achieve a better vacuum level. The minimum vacuum level able to be achieved by the diffusion pump is about 4.0×10^{-5} mbar within two hours of the pumping. After that, the high vacuum valve is closed and the roughing valve is opened to continue the pumping process. The bottom electrode, which acts as substrate holder, is heated to the desired temperature as substrate temperature for the deposition. The substrate temperature is dependent on the voltage supply to the temperature controller by Regavolt. In this work, voltage of 120 V is enough to achieve a substrate temperature of 300°C and is also calibrated for the substrate temperature below 300°C. The system is

ready for the deposition process at the required temperature when the temperature is reached. Another very important safety procedure is purging the SiH_4 gas line with purified nitrogen (PN) gas to remove air or any excess SiH_4 gas from the line. Purging the system can prevent vapour condensation, decomposition and explosion of hydrocarbon pump oil. Besides, the PN is also used to clean the substrate in the reaction chamber before the deposition.

Before SiH_4 is allowed to flow into the reaction chamber, the PN gas tank (nitrogen gas labelled as 5 in the Figure 3.2) is opened and the gas pressure is controlled at a fixed pressure of 60 psi to operate the safety system, and this will automatically turn on the pneumatic valve and allow the SiH_4 gas to flow through it. The excess flow switch (EFS) is utilized in the gas line to stop any uncontrollable excess SiH_4 gas from flowing through. The EFS will activate if the pressure inside this line is suddenly increased above 70 psi and the alarm in the safety system will ring. At the same time, nitrogen gas labelled as 1 in Figure 3.2 is allowed to flow into the gas inlet of the roughing pump, which will dilute the excess SiH_4 gas when deposition starts. The flow of SiH_4 gas into the system is initiated by opening the SiH_4 gas tank. The valve is opened until the gas pressure reaches 100 psi and the valve is closed. This is for safety issues, in order to prevent more SiH_4 from flowing into the gas lines and also to reduce the excess SiH_4 gas from the gas line. The SiH_4 gas regulator is set to 30 psi to control the gas flow into the gas line. The H_2 gas is allowed to flow into the reaction chamber by opening the valve of the H_2 gas tank and gas pressure is monitored by a regulator at about 100 psi. The flow of the SiH_4 and H_2 gases into the reaction chamber is finally monitored accurately by a mass flow controller.

The deposition process proceeds when the required rf power is applied across the electrodes (showerhead electrode). The rf power is maintained by tuning the matching impedance with zero reflected power throughout the deposition process. The

deposition time is measured from the moment when the rf power supply is maintained at a desired rf power. The LBL deposition technique here is performed by periodically alternating the deposition of the film layer for 5 minutes with hydrogen plasma treatment on the growth surface for 3 minutes. This process was repeated for four cycles, producing four periodic layers of the film deposited intermittently with hydrogen plasma treatment of the growth surface, resulting in a total deposition time of 32 minutes. This LBL mode was performed by switching off the silane source at the end of each cycle of film layer deposition, followed by hydrogen plasma treatment of the deposited surface. The maximum delay time for the switching time is less than 0.5 second. The CD deposition technique is a continuous deposition without interruption of hydrogen plasma treamtment for a toral deposition time of 32 minutes. For both deposition techniques, hydrogen plasma cleaning of the chamber and substrates was performed for 10 minutes prior to the deposition process. The power for generating the hydrogen plasma cleaning is fixed at 40 W. During the deposition processes, the parameters such as the deposition pressure, substrate temperature, rf power, SiH_4 and hydrogen gases flow-rates must be carefully monitored and maintained throughout the deposition process. The roughing valve shown in Figure 3.2 is used to maintain the gas pressure in the reaction chamber to the desired deposition pressure. When the deposition is completed, the rf power supply is turned off.

In this work, the deposition pressure was fixed at 0.8 mbar. Three sets of samples were deposited on c-Si and glass substrates for both the LBL and CD films. These sets of films consisted of the films deposited at different rf powers, substrate temperatures, T_s and hydrogen to silane flow-rate ratios, R. Table 3.1 tabulates the deposition parameters used for depositing these sets of LBL and CD films. The c-Si substrate is p-type c-Si wafer with orientation of (111) plane and resistivity of about 1-10 Ωcm. The c-Si with p-type and orientation of (111) give to minority carriers of

electron for electrical measurement and enhancement of the film growth in preferred orientation of (311) plane, respectively. The corning glass substrate is high purity silicon dioxide with a low thermal expansion coefficient.

Table 3.1: Deposition parameters of Si:H films deposited by LBL and CD deposition techniques at different rf powers, substrate temperatures, T_s and hydrogen to silane flow-rate ratios, R.

Deposition Parameters	rf power (W)	Substrate temperature, T_s (°C)	Hydrogen to silane flow-rate ratio, R
Set 1 (LBL, CD)	20, 40, 60, 80, 100	300	20
Set 2 (LBL, CD)	40	RT, 100, 200, 300, 400	20
Set 3 (LBL, CD)	40	300	2, 4, 8, 12, 16, 20

The rationale of choosing the range of the deposition parameters is followed the optimized deposition parametes from previous published works (Shi et al., 2006; Shi et al., 2007).

At the end of the deposition, the rf power applied to the top electrode (showerhead) is turned off by adjusting to zero power. The gas line is pumped down until the pressure reaches the pre-deposition pressure of 2.0×10^{-3} mbar. This can also be confirmed by monitoring the mass flow controller, which shows a zero flow-rate reading for all gases. Consequently, this can certify that there are no excess gases left in the gas line. The valve leading to the reaction chamber is closed and the bypass is opened to allow the gas line to be purged with purified nitrogen gas (with the labelled as 3 in Figure 3.2) for several cycles, where each cycle time is about 10 minutes. Each purging cycle will flush out any excess SiH_4 gas and remove any contaminants in the gas line. These gases are allowed to flow into the roughing pump and exhaust lines through the roughing pump outlet.

The purging technique is necessary not only for the post deposition process, but also when the system is not used for a long period of time. The purging process, where purified nitrogen is allowed to flow through the system for a considerable period of time, may leave unacceptable levels of air and moisture in the system. A much more efficient technique is cyclic variation in pressure, preferably pressurization followed by

evacuation. The evacuation and purge operation is repeated several times, where each cycle time lasts about 10 minutes. The high pressure of PN which is about 20 psi (100 kPa) is found to be the most practical pressure used to purge the gas lines.

3.3 Analytical Techniques

In this work, there are various characterization techniques employed on Si:H thin films deposited by LBL deposition technique to study the optical, structural, crystallinity and surface morphology properties of the films. These characterization techniques include optical transmission spectroscopy (Ultra-violet visible near-infrared), Fourier transform infrared (FTIR) spectroscopy, X-ray diffraction (XRD), Micro-Raman scattering spectroscopy, Photoluminescence (PL) spectroscopy, field emission scanning electron microscopy (FESEM) and high resolution transmission electron microscopy (HRTEM). In order to obtain the parameters that represent the properties of the films, there are several calculation techniques corresponding to every characterization technique that will be described in this section.

For measurement purpose, the films for this study have been deposited on two kinds of substrates, which are crystal silicon (c-Si) and Corning glass substrates. The films deposited on c-Si substrate were used for most of the characterization techniques, such as FTIR spectroscopy, XRD, Micro-Raman scattering spectroscopy, PL spectroscopy, FESEM and HRTEM. While the films deposited on glass substrate were used for optical transmission spectroscopy, XRD and Micro-Raman scattering spectroscopy.

The various optical parameters such as film thickness, refractive, n and optical energy gap, E_G are determined from the optical transmission spectrum of the film. The hydrogen content, C_H and microstructure parameter, R which represents the structural properties of the film obtained from FTIR spectrum. The XRD spectrum is used to

estimate the crystallite size in the film through Scherrer equation, which will be explained in detail in this topic. The crystallinity or crystalline volume fraction, X_C of the film is estimated from Raman scattering spectrum. Finally, the distribution of particles appears on the film and the size of nanocrystallites embedded within amorphous matrix is measured by FESEM and HRTEM respectively.

3.3.1 Optical Properties

3.3.1.1 Experimental Determination of the Refractive Index and Film Thickness

For the experimental determination, the optical functions of the film on transparent substrate are determined from the optical transmission spectrum, $T(\lambda)$ measured by optical spectrophotometer. From the optical transmission spectrum, we have used methods proposed by Manifacier et *al*. and Davies et *al*. to determine the refractive index and film thickness of the film, respectively. The following paragraphs give the important optical relations developed by Manifacier group under certain assumptions, as they constitute the theoretical basis of the numerical determination of the optical parameters used in this topic.

The optical response of the film is expressed as follows in terms of the refractive index, n, and the extinction coefficient, k.

$$\tilde{n}(\lambda)=n(\lambda)-ik(\lambda), \tag{3.2}$$

When considering a uniform homogeneous thin film with film thickness, d, and optical functions n (λ) and $k_1(\lambda)$ on a transparent (k_2=0) thick substrate with refractive index $s(\lambda)$ (Corning glass in our experiment), no coherent multiple reflections take place in the substrate. A parallel beam of light with wavelength λ is incident normally on the film-substrate system. If d and λ are of the same order of magnitude, interference will be observed in both transmission (T) and reflection spectra (R). In the weak absorption region, the T of film at λ is expressed as follows (Manifacier *et al.*, 1976):

$$T = \frac{I_T}{I_o}, \qquad \text{Ratio of intensity transmitted to intensity incident}$$

$$= \frac{(1-R_1)(1-R_2)(1-R_3)\,exp(-\alpha d)}{(1-R_2R_3)\left\{1-\left[R_1R_2 + R_1R_3(1-R_2)^2\right]exp(-2\alpha d)\right\}}, \tag{3.3}$$

where I_o, I_T is the incident and transmitted light respectively, R_1, R_2 and R_3 are the reflectance at air-film, film-substrate, and substrate-air interfaces, respectively. α is absorption coefficient of the film.

The reflectance spectra, R at the interfaces are expressed as:

$$R_1 = \frac{(n-n_o)^2}{(n+n_o)^2}, \tag{3.4}$$

$$R_2 = \frac{(n-n_1)^2}{(n+n_1)^2}, \tag{3.5}$$

$$R_3 = \frac{(n_1-n_o)^2}{(n_1+n_o)^2}, \tag{3.6}$$

where n, n_o and n_1 are indices of reflection for film, air and Corning glass respectively.

Figure 3.4 illustrates the beam path of light incident on a Si:H thin film. The reflection at the air and film interface, film and substrate interface, substrate and air interface, and the absorption by film have strong influence on the optical transmission spectrum. A typical transmission spectrum for the film is shown in Figure 3.5.

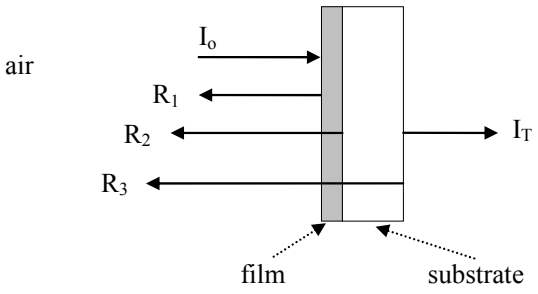

Figure 3.4: Transmission of light passing through a Si:H thin film. I_o and I_T are the intensities of incident and transmitted light respectively. R_1, R_2, and R_3 are the reflected light at the air-film, film-substrate and substrate-air interfaces, respectively.

From Figure 3.5, the spectrum shows consistent interference pattern at the higher wavelength region (in the transparent region). The maxima (T_{max}) and minima (T_{min}) of each interference fringe are measured by enveloping the spectrum in the transparent region as shown in the figure.

The refractive index n of film is expressed by the equations proposed by Manifacier *et al.*:

$$n = \left(N + \left(N^2 - n_o{}^2 n_1{}^2 \right)^{1/2} \right)^{1/2}, \tag{3.7}$$

Where $$N = \frac{n_o{}^2 + n_1{}^2}{2} + 2 n_o n_1 \frac{T_{max} - T_{min}}{T_{max} T_{min}}, \tag{3.8}$$

n_o is the refractive index of air; 1.00 and n_1 is the refractive index of Corning glass; 1.52.

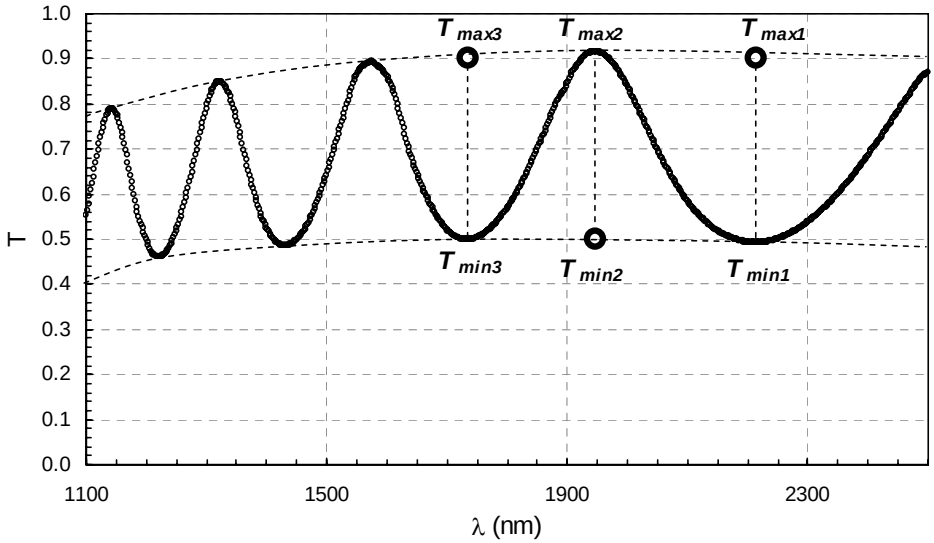

Figure 3.5: The transmission curve with envelope functions of T_{max} and T_{min} (The data is provided from the film deposited at hydrogen to silane flow-rate ratio, R, rf power and substrate temperature, T_s of 20, 40 W and 100°C respectively).

The optical thickness can be obtained by varying the interference order, *m* until it fits the linear relation between *nd* and λ, which are proposed by Davies *et al*. using the expression:

$$m\lambda = 2nd \,, \tag{3.9}$$

where λ, *n* and *d* are the wavelength, refractive index and optical thickness of the selective order, respectively.

The *m* is smallest for the first maximum or minimum point at the longest wavelength and increases by half for each consecutive maximum or minimum point. But the *m* must be in integer where *m* = 1, 2, 3… for maxima and *m*' = *m* + ½ for minima. By starting off with the order of the first optimum point as one, a plot of $\frac{m\lambda}{2} = nd$ versus λ is obtained. If the plot does not replicate an exponentially decreasing plot, the value of *m* at the first maximum or minimum point at the longest wavelength is increased by one. This procedure is repeated until the required plot is obtained. The value of *m* producing the required plot is obtained (Figure 3.6). The value of *m* producing the required plot produces the correct order for the interference fringes. From equation (3.9), the values of *nd* can be determined using the correct *m* value. Using the refractive index obtained at the longest wavelength obtained by Manifacier technique, the film thickness is determined at this wavelength. Since thickness is the same for all wavelengths, this value of thickness is taken to be the film thickness. The *n* values at different wavelength positions of the maximum and minimum peaks on the spectrum are then determined using this thickness. These values are them fitted to Cauchy function (Klein and Cogan, 1990):

$$n = \frac{a}{\lambda^2} + n_o' \,, \tag{3.10}$$

where *a* is a constant characteristic of the dispersion of the refractive index and n_o' is the static refractive index value of the film.

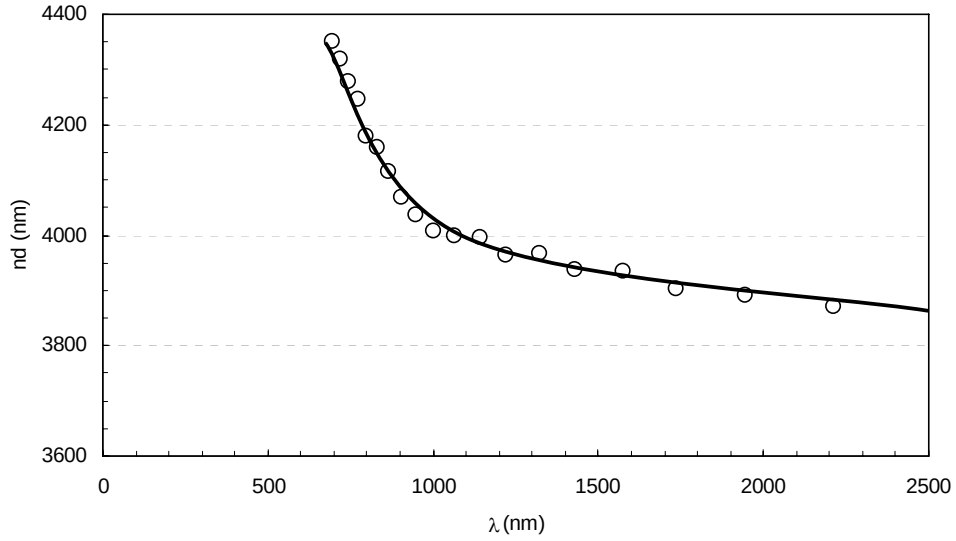

Figure 3.6: Variation of *nd* against λ (The data is provided from the film deposited at *R*, rf power and T_s of 20, 40 W and 100°C respectively).

3.3.1.2 Optical Absorption and Optical Energy Gap

From the transmission and reflection data, the absorption coefficient of the thin film, α is determined by the following expression:

$$\alpha = \frac{1}{d} ln\left(\frac{1-R}{T}\right), \tag{3.11}$$

where *d* is the thickness of the thin film.

The optical energy gap, E_G is the energy differences between the maximum of the extended states in the valence band and the minimum of the extended states in the conduction band. In other words it represents the minimum energy for transition of electrons between these states. From the α above, the E_G of the film is determined from Tauc relation (Tauc and Abeles, 1972; Tauc, 1974):

$$\alpha E = B\left(E - E_G\right)^{\varphi}, \tag{3.12}$$

where *B* is a constant, *E* is the photon energy, φ = ½ for a directly allowed transition and φ = 2 for an indirectly allowed transition.

For the Si:H thin film, which is considered as an indirect semiconductor, using the Tauc relation (Tauc and Abeles, 1972; Tauc, 1974) as described in Section 2.7.1:

$$\left(\alpha E\right)^{1/2} = B^{1/2}\left(E - E_G\right), \tag{2.5}$$

By plotting the graph $(\alpha E)^{1/2}$ against photon energy, E as shown in Figure 3.7. The E_G can be obtained from the intersection of the linear part of the curve extrapolated onto the energy axis.

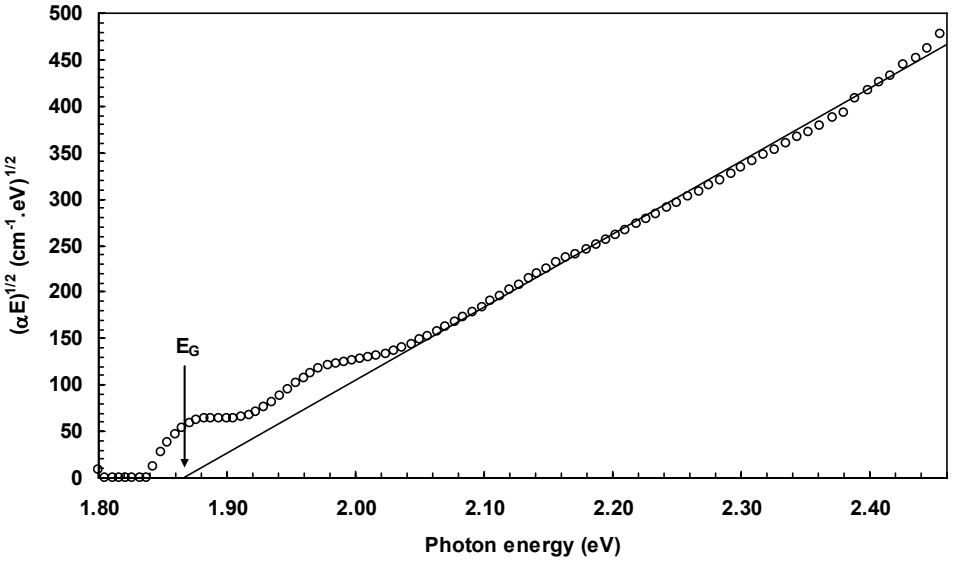

Figure 3.7: A typical plot of optical absorption edge (The data is provided from the film deposited at R, rf power and T_s of 4, 40 W and 300°C respectively).

3.3.2 Fourier Transform Infrared (FTIR) Spectroscopy

Infrared (IR) absorption spectroscopy is the most direct information, which can indicate the local bonding environment of the constituent atoms and hence the molecular structure in the deposited films, especially the bond of silicon and hydrogen. All the vibration modes in amorphous semiconductors are optically active. They can be divided into low frequency acoustic modes, intermediate frequency bond bending modes, and lastly, high frequency bond stretching modes. The frequency of the mode is

determined by the nearest neighbor's interactions and their relative activity by local molecular symmetry.

3.3.2.1 Theoretical Background

This technique involves the passage of a long wavelength infrared beam through a film deposited on a substrate, which is transparent to infrared light. The transmitted signal intensity through a depth is given by (Vickerman, 1997),

$$\frac{I_o}{I_t} = exp(-kcl), \tag{3.13}$$

where I_o is the intensity of the incident light on the film; k the absorption coefficient that is the imaginary part of the complex function refractive index, $\tilde{n}$ and c is the concentration of the absorbing material and $\frac{I_o}{I_t}$ is known as the transmittance, T.

For the quantitative analysis, the transmittance of the film was given by the ratio of the transmittance spectrum of the film on the substrate and the transmittance spectrum of the substrate.

3.3.2.2 Silicon-Hydrogen Bonding Configurations

A typical IR spectrum of Si:H thin film deposited on high-resistivity crystalline silicon substrates, which are transparent in the IR regime, is shown in Figure 3.8. This spectrum is in the scanning range of 4000 to 400 cm^{-1} where the silicon-hydrogen vibrations are absorbed. This spectrum presents the various types of Si-H bonds, their vibrational modes and wavenumbers of the infrared absorptions which correspond to them. The absorption near 640 cm^{-1} relates to Si-H wagging mode (Lucovksy *et al.*, 1979). The peaks at 845 cm^{-1} and 885 cm^{-1} correspond to the same vibrational mode as $Si-H_2$ bending modes (Knights *et al.*, 1981). The peaks at 2000 – 2090 cm^{-1} correspond to Si-H and $Si-H_2$ stretching bands, which are located at around 2000 cm^{-1} and 2090 cm^{-}

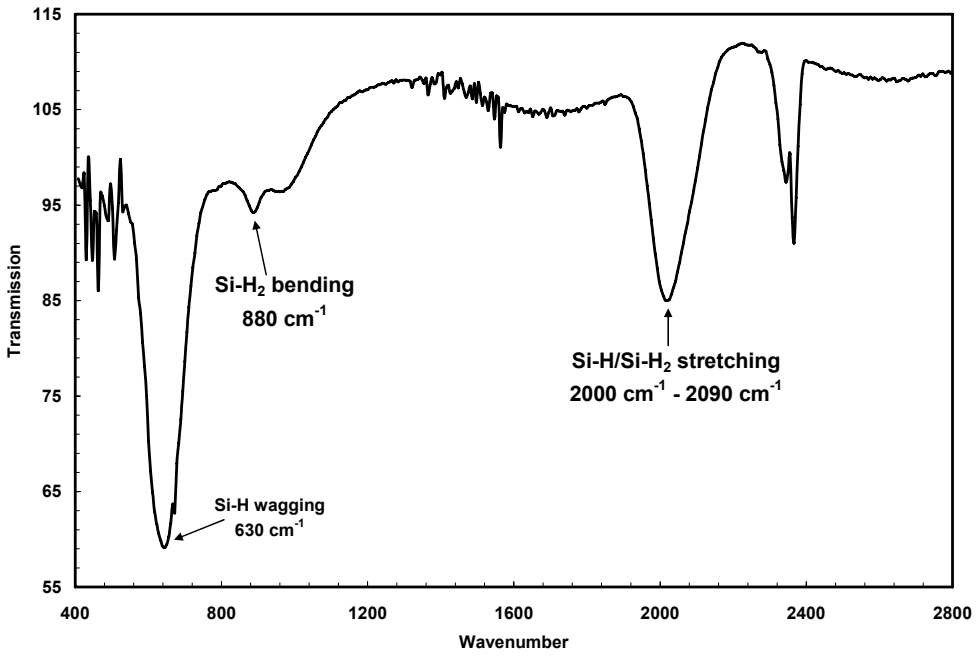

Figure 3.8: A typical infrared transmission curve of Si:H thin film obtained by conventional FTIR spectrometer (The data is provided from the film deposited at R, rf power and T_s of 20, 40 W and 300°C respectively).

[1], respectively (Brodsky *et al.*, 1977). A considerable effect of air exposure is that the absorption peak at 1,200-800 cm^{-1}, which is associated to Si-O, -C, and –N bonding are due to the contaminants on the surface layer (Talukder *et al.*, 1993). The amount of oxygen in the form of Si–O bonds can also be noticed in PECVD Si:H thin films (Lucovsky *et al.*, 1983; Masson *et al.*, 1987; Ruther, and Livingstone, 1994). Figure 3.9 shows the example of various vibrational modes of silicon-hydrogen bonding and their direction of the bonding (Searle, 1983).

3.3.2.3 Hydrogen Content, C_H and Microstructure Parameter, R Determination

The analysis of infrared absorption spectra is used to determine the bonded hydrogen content and the microstructure content in the film. From the FTIR spectrum of Si:H thin film in Figure 3.8, the hydrogen content, C_H can be determined from the integrated intensity of the wagging band that occurs at the wavenumber of 630 cm^{-1}. While the microstructure parameter, R can be determined from the integrated intensity

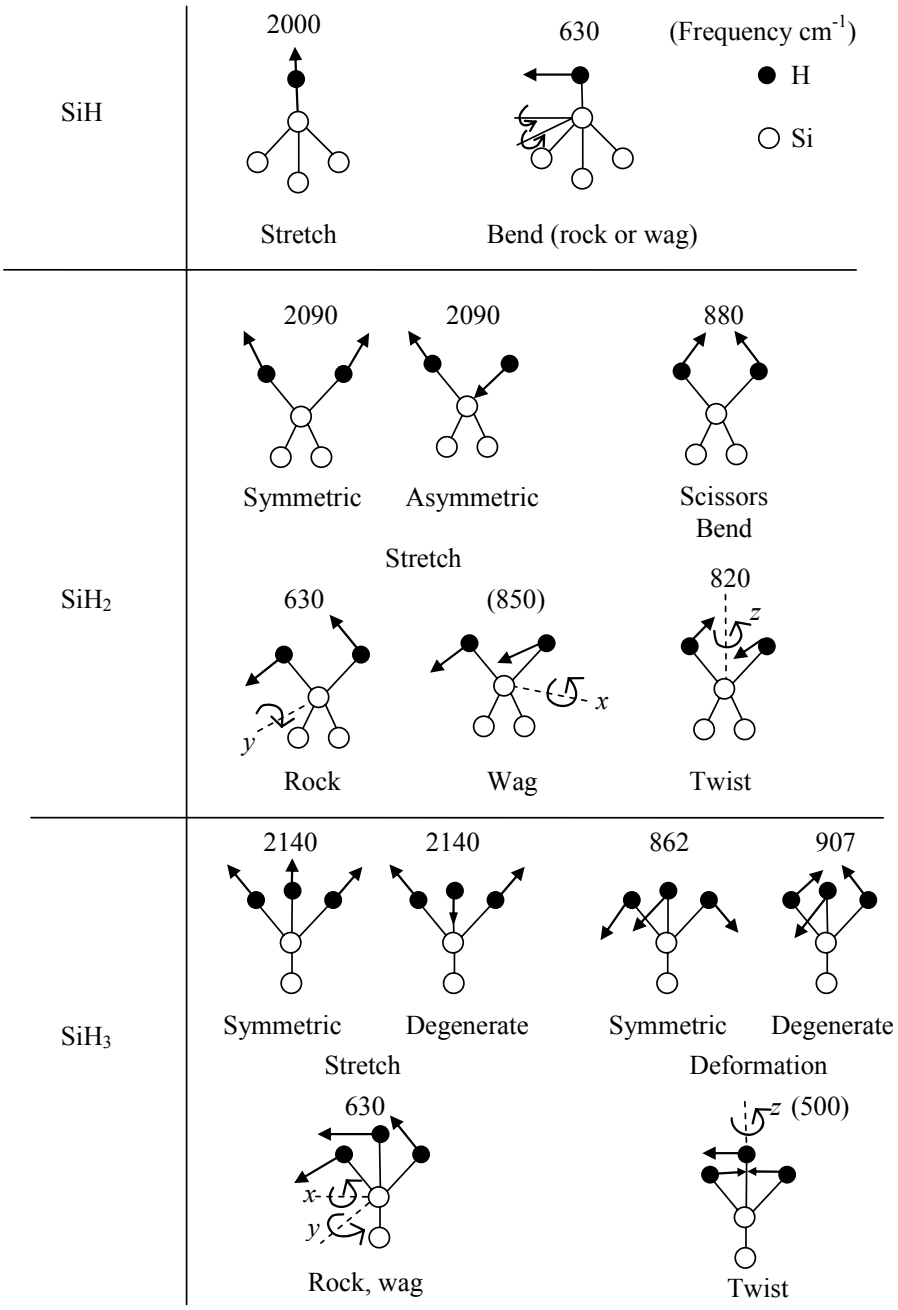

Figure 3.9: The set of Si-H vibrational modes for SiH, SiH_2 and SiH_3 groups, with calculated frequencies as indicated. The frequencies in brackets are estimates.

of two stretching bands that occur at wavenumber of 2000 cm^{-1} - 2100 cm^{-1}. The details of calculation techniques of these two important parameters representing the structural properties of the film will be shown below.

From the transmission spectra, the spectrum around the peaks at 630 cm^{-1} and 2000 cm^{-1} - 2090 cm^{-1} are converted into absorption coefficient spectra using the relationship (Saadah, 2001),

$$\alpha(\omega) = \frac{1}{d} ln\left(\frac{100}{T\%}\right), \tag{3.14}$$

where d is the thickness of the film.

The integrated intensity of the absorption peak representing a bonding configuration is (Cardona, 1983):

$$I = \int \frac{\alpha(\omega)}{\omega_o} d\omega, \tag{3.15}$$

where α and ω_o are the absorption coefficient and the wavenumber of absorption peak, respectively.

The Gaussian or Doppler lineshape is used to deconvolute component peaks from the absorption spectrum (Kniffer *et al.*, 1983; Shanks *et al.*, 1980).

The general equation used for Gaussian lineshape is:

$$\alpha(\omega) = \alpha(max) exp\left\{-\frac{4(ln2)(\omega-\omega_o)^2}{(\Delta\omega)^2}\right\}, \tag{3.16}$$

where $$\alpha(max) = \frac{2(ln2)^{1/2} S_{band}}{\pi^{1/2}\Delta\omega}, \tag{3.17}$$

and $$S_{band} = \int \alpha(\omega) d\omega, \tag{3.18}$$

where $\alpha(max)$, S_{band}, $\Delta\omega$ and ω_o are the maximum absorption coefficient, the area under the curve of the absorption peak, the full width half maximum (FWHM) of the absorption peak and the position of absorption peak, respectively.

Using Equation (3.15), the integrated intensity can be expressed as:

$$I = \frac{S_{band}}{\omega_o}, \tag{3.19}$$

where S_{band} and ω_o can be determined after the fitting using Gaussian deconvoluted method.

For the wagging band centered on 630cm^{-1}, the atomic density of H was obtained from the expression (Ruther and Livingstone, 1994),

$$N_H = A\int\left[\frac{\alpha(\omega)}{\omega_o}\right]d\omega, \qquad \text{or} \qquad \frac{AS_{band}}{\omega_o}, \tag{3.20}$$

where A is proportionality constant, 1.60×10^{19} cm^{-2} (Langford *et al.*, 1992).

The hydrogen atomic concentration, C_H is expressed as atomic percentages (Han and Wang, 2003),

$$C_H = \frac{N_H}{N_{Si}}\times100\%, \tag{3.21}$$

where N_{si} is the atomic density of silicon (5×10^{22}cm^{-3}) (Shanks *et al.*, 1980).

Furthermore, the R in the film can be determined using the relation below (Bhattacharya and Mahan, 1998):

$$R = \frac{I_{2090}}{I_{2000} + I_{2090}}, \tag{3.22}$$

where I_{2000} and I_{2090} are integrated intensity of Si-H stretching band at 2000 cm^{-1} and integrated intensity of Si-H_2 stretching band at 2090 cm^{-1} , respectively, which can be obtained by using equation (3.14-3.19).

Figure 3.10 shows the example of Gaussian fitting for the infrared absorption peaks of Si:H thin film located at around 630 cm^{-1} and 2000-2090 cm^{-1}. The Gaussian fitting components were fitted by using Origin Pro version 8.1.

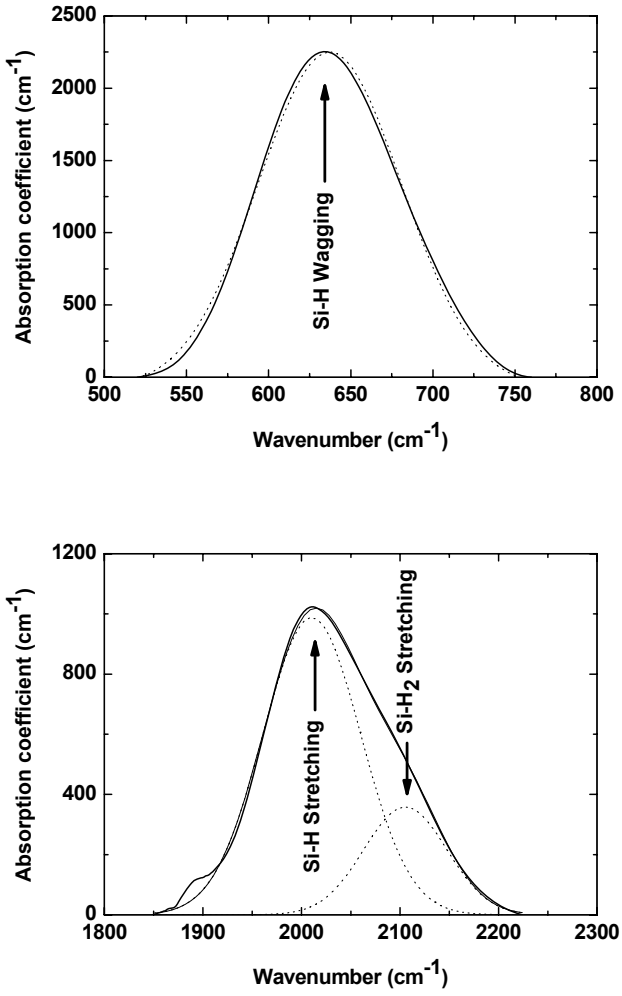

Figure 3.10: A typical selected infrared transmission curve of Si:H thin film and its deconvolution fitting using Gaussian method (The data is provided from the film deposited at R, rf power and T_s of 20, 40 W and 300°C respectively).

3.3.3 X-Ray Diffraction (XRD)

X-Ray Diffraction (XRD) measurement is the most powerful and commonly used technique as it can provide information about phase identification, chemical composition and crystallite size (Coscia *et al.*, 2003; Zhao *et al.*, 2005). It can also be used for quantitative analysis of phase compositions and crystallinity in the film structure and its orientation (Lee and Singh, 1999). The XRD pattern can be detected from a diffracted beam, which is composed of many waves that have been scattered by atoms in a crystal that were in the path of the incident beam. Reflection is the bouncing

back of visual light as a surface phenomenon in a layer. The diffraction of waves only occurs at certain angles, called Bragg angles, where Bragg's law is satisfied. In contrast, reflection takes place at any angle of incidence as illustrated in Figure 3.11(a). The value of interplanar spacing, d and the number and types of atoms in each plane are unique for every mineral.

The unit operates through the diffraction of radiation emanating from the line of focus at the sample and then recorded by the detector. The diffracted beam path is shown in a schematic diagram of an X-ray diffractometer in Figure 3.11(b). There are two different diffraction geometries that have been used for characterization of the measuring sample, which are the Bragg-Brentano (BB) and the Thin-Film configurations. In this work, the Thin-Films configuration has been chosen for investigating phase transition of the Si:H thin film. This technique is called asymmetric diffraction geometry because the angles of the incident beams with respect to the sample surface are different. The angle θ between incident radiation and the film surface is kept constant at a very small value (usually less than 5 ^{o}) and the detector is moved varying the detection angle. In this configuration, only the diffraction from crystallographic planes, which are not parallel to the samples, is registered at any diffraction angle. However, the volume of material contributing to the diffraction is relatively large, and remains almost constant during the whole measurement. This is because the angle of incidence of the primary beam is low and fixed, and the irradiated area on the sample surface is larger than the BB configuration. For this reason, this configuration is more suited for studies of thin films, where the intensity of reflections is often very small. If the angle of incidence of the primary beam is very low, its path in the film will be long and the penetration of the beam will be very low thus giving high intensity to contribution from the film surface. The X-ray radiation used for XRD is in the wavelength spectral range of 0.5-2.5 Å, which corresponds to the energy spectral

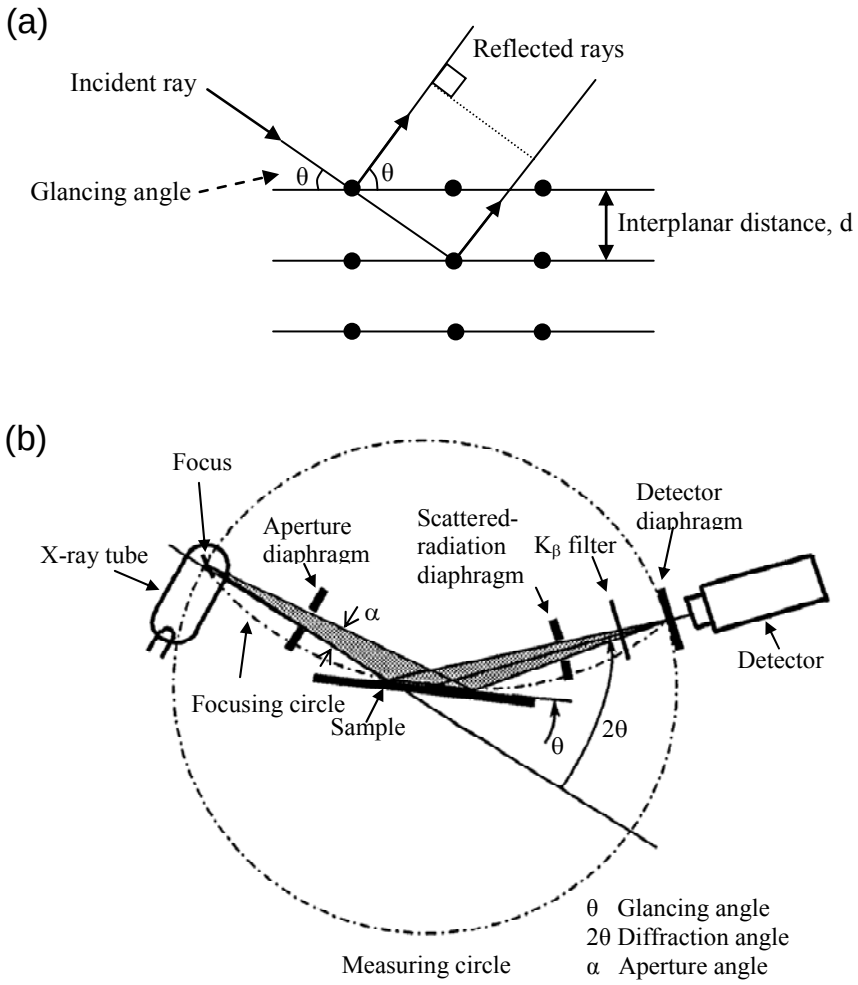

Figure 3.11: (a) The principle of X-ray diffraction and (b) X-ray diffracted beam path in θ/2θ mode.

range of 5-20 KeV. The typical penetration depth of X-ray in the matter is in the order of 100 μm.

According to the Scherrer equation (Klug and Alexander, 1985), the average grain size *D* of a sample measured by XRD can be estimated using:

$$d = 0.9\lambda / B\cos\left(\theta_B\right), \tag{3.23}$$

where 0.9, λ, B, θ_B are the Scherrer's constant, wavelength of Cu-K_α X-ray source (λ=1.5402Å), full width of half-maximum (*FWHM*) of the diffraction peak and the peak position at $2\theta_B$, respectively.

Figure 3.12 shows a typical XRD spectrum of nc-Si:H film (Torchynska *et al.*, 2008). As can be seen in the figure, the spectrum demonstrates the broad peak at around 22 ^{o} that deals with a-Si:H. Besides, the spectrum also consists of sharp peaks at $2\theta =$ 28.4 ^{o}, 47.4 ^{o} and 56 ^{o} (peak I, II and III) that correspond to (111), (220) and (311) silicon crystal planes, respectively (Torchynska, 2009). The peak at I actually can be decomposing to two signals (labelled as 1 and 2) related to Si nanocrystals with different sizes. From the literature, usually the biggest NCs (1) are characterized by the size in the range of 10 nm – 30 nm and smallest NCs (2) have sizes of 2 nm – 8 nm (Torchynska *et al.*, 2008). Figure 3.13 shows an example of the decomposition of XRD peaks at 28 ^{o} using Gaussian multi peaks fitting (a) and Gaussian single peak fitting (b).The Gaussian multi peaks fitting is needed for the film consisting of two difference sizes of nanocrystals. These multiple peaks fitting can be done by using Origin Pro version 8.1.

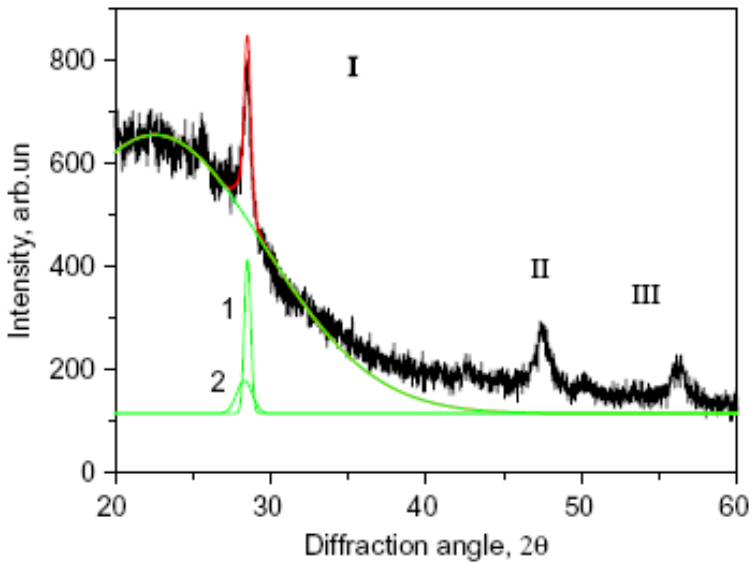

Figure 3.12: Decomposition of the peak at 28 ^{o} in the XRD spectrum.

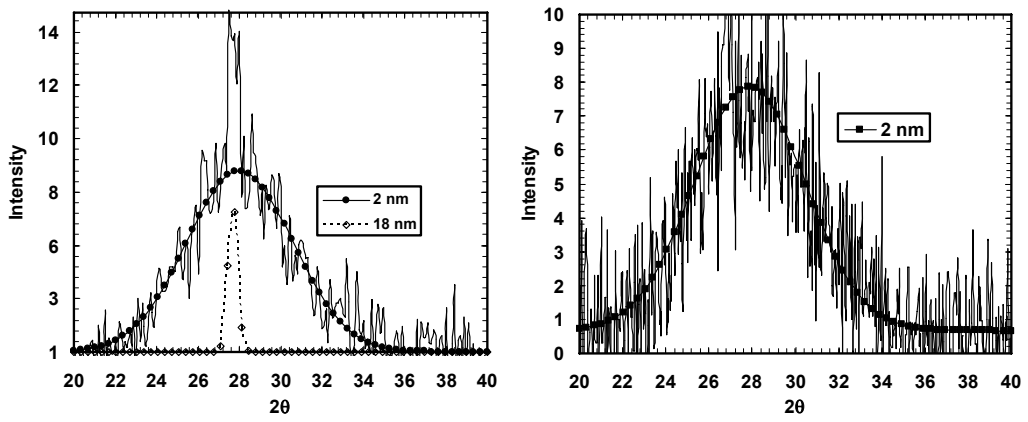

Figure 3.13: Decomposition of the peak at 28 ^{o} in the XRD spectrum using Gaussian multi peaks fitting (The data is provided from the film deposited at *R*, rf power and T_s of 12, 40 W and 300°C respectively). (The data is provided from the film deposited at *R*, rf power and T_s of 20, 100 W and 300°C respectively).

3.3.4 Micro-Raman Scattering Spectroscopy

Raman spectroscopy is based on the Raman Effect, which consists of the inelastic scattering of photons by the sample. When light is incident on a sample, most of the light is elastically scattered in random directions. This phenomenon is known as Rayleigh scattering. However, there is a small remaining fraction of the light that is inelastically scattered, a phenomenon which is known as Raman scattering. The inelastically scattered light has a wavelength higher or lower than the one of the incident light. The difference in energy is due to rotational and vibrational transitions in the material target. This shift in photon energy corresponds to the energy of phonons that have been created or annihilated according to the energy and momentum conservation rules (Laidler and Meiser, 1995):

$$\omega_s = \omega_i \pm \Omega , \tag{3.24}$$

$$\vec{q_s} = \vec{q_i} \pm \vec{K} , \tag{3.25}$$

where ω_i and ω_s are the incident and scattered photon frequencies respectively, $\vec{q_i}$ and $\vec{q_s}$ are the incident and scattered photon wavevectors, respectively, and Ω and $\vec{K}$ are

the phonon frequency and wavevector, respectively.

When the photon loses energy into the creation of a phonon, it is called Stokes scattered, and when it gains energy from the annihilation of a phonon, it is called anti-Stokes scattered. Since Raman scattering is inherently a weak process, a high power light source, such as a laser is usually required to obtain a measurable scattered intensity. Also, extremely sophisticated spectrometers are needed in order to probe into the properties of the material, such as phase state, degree of crystallinity and crystal size among others.

Figure 3.14 shows a typical Raman spectrum from nc-Si:H film, which can be divided into four bands corresponding to four kinds of phonon modes, i.e., a transverse acoustic (*TA*) brand with a peak at 150 cm^{-1}, a longitudinal acoustic (*LA*) mode with a peak at 300 cm^{-1}, a longitudinal optical (*LO*) branch with a peak at 380 cm^{-1} and transverse optical (*TO*) mode (Gullanar *et al.*, 2003; Zhang *et al.*, 2004; Wei *et al.*, 2007). Furthermore, the *TO* band can be further divided into two components: a transverse optical (TO_1) branch with a peak at 480 cm^{-1} from the amorphous Si component and another transverse optical (TO_2) mode at 510 cm^{-1} – 520 cm^{-1} from the contribution of Si nanocrystals (Gullanar *et al.*, 2003; Wei, 2007). These modes are depicted in the figure in which the *TA*, *LA*, *LO* and TO_1 branches can be fitted well with Gaussian line respectively. This illustrates that every fitted line can be approximately represent every mode deconvoluted from an experimental Raman spectrum.

The theoretical calculation of the Raman spectra give detailed information of structural properties of nc-Si:H film. Due to the asymmetry of the TO_2 crystalline peaks, the strong phonon confinement (SPC) model, which has been widely used in polycrystalline and microcrystalline materials, is employed. According to this model, the Raman red-shift and line broadening are attributed to the confinement of optical phonons in a small crystalline particle. When the size of the particles reduced to the

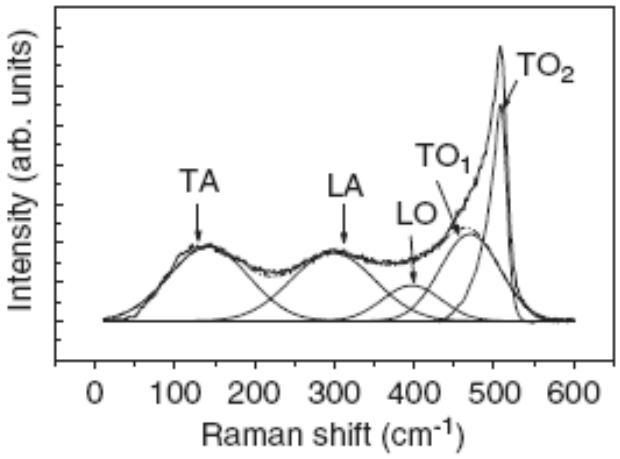

Figure 3.14: A typical Raman spectrum of nc-Si:H film. The spectrum can be deconvoluted into *TA*, *LA*, *LO*, *TO1* and *TO2* modes as described in text.

order of nm, the wave function of optical phonons will no longer be a plane wave. The localization of wave function leads to a relaxation in the selection rule of wave vector conservation, resulting in the red-shift of the peak position. Square of Fourier transform (Gullanar *et al.*, 2003),

$$\left|C(q)\right|^2 = \exp\left(-q^2L^2/16\pi^2\right), \tag{3.26}$$

gives the scattering probability of phonons with the different wave vector q, where L is the correlation length related with the grain size.

The first-order Raman spectrum is then given by (Richter *et al.*, 1981; Campbell and Fauchet, 1986):

$$I(\omega) \cong \int_0^{2\pi/a_0} \frac{\left|C(q)\right|^2 4\pi q^2 dq}{\left[\omega_0 - \omega(q)\right]^2 + (\Gamma/2)^2}, \tag{3.27}$$

where ω_0 = 521.5 cm^{-1}, a_0 = 0.5483 nm is the lattice constant of the bulk Si crystal, Γ is the line-width of the phonon in the bulk Si (3.6 cm^{-1}, including instrumentation broadening).

The phonon dispersion relation is taken according to (Tubino *et al.*, 1972):

$$\omega(q) = \left[A + B\cos(\pi q / 2) \right]^{1/2}, \tag{3.28}$$

where A = 1.714×10^5 cm^{-2} and B = 1.0×10^5 cm^{-2}, the value obtained experimentally by neutron scattering (Tubino *et al.*, 1972).

The average crystallite size can be relate followed by,

$$d = \frac{L}{a_o}, \tag{3.29}$$

Due to the two-phased structure of nc-Si:H thin films, elastic tensile strain may exist in the area between disordered amorphous tissue and nanocrystalline grains. By considering the phonon confinement effect and an additional red-shift $\Delta\omega$ caused by the effect of tensile strain simultaneously, the Raman spectrum can be fitted and reconstructed as shown in Figure 3.15.

From the Gaussian fitting in Figure 3.15, the crystalline volume fraction, X_C can be estimated as following equation (Gajovic *et al.*, 2009):

$$X_C = \frac{I_{520} + I_{500}}{\beta I_{480} + I_{520} + I_{500}}, \tag{3.30}$$

where I_{520}, I_{500} and I_{480} are integrated intensities of the Raman peaks corresponding to crystalline component, grain boundaries and amorphous component, respectively.

The factor β is the ratio of the cross-section of the amorphous phase to the crystalline phase, and is defined as (Das, 2005):

$$\beta = 0.1 + \exp(-d / 250), \tag{3.31}$$

where d is the grain size in nm. In the case of the μc-Si and nc-Si films, with their small crystallites, β is ≅ 1.

Furthermore, the average crystallite size, d can be estimated from the shift of the crystalline peak using following equation (Cardona and Guntherodt, 1982):

$$d = 2\pi(B / \Delta\omega)^{1/2}, \tag{3.32}$$

where B is a constant valued of 2.21 $nm^2.cm^{-1}$, $\Delta\omega$ is the peak shift, the deviation of the measured crystalline peak location from the c-Si peak at 521.5 cm^{-1} as suggested by Tsu *et al*.

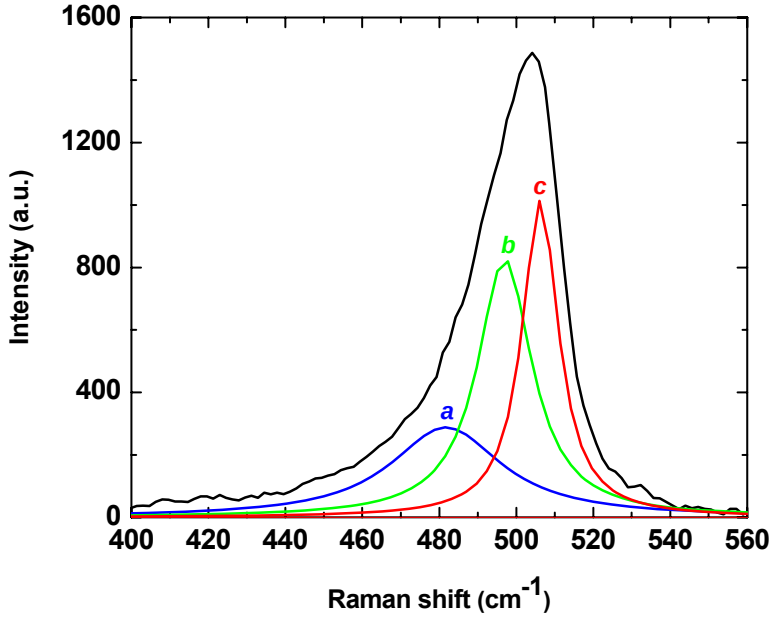

Figure 3.15: Lorentzian deconvolution of Raman peak at around 500 cm^{-1} of the films deposited at different substrate temperatures. The line shapes of the three satellite components are indicated by ***a***, ***b*** and ***c,*** which corresponds to amorphous, grain boundaries and crystalline components (The data is provided from the film deposited at R, rf power and T_s of 20, 40 W and RT respectively).

3.3.5 Micro-Photoluminescence (PL) Spectroscopy

Photoluminescence (PL) spectroscopy is a powerful tool used to characterize the optical property of semiconductors. It is a simple, versatile, contactless and nondestructive method of probing the electronic structure of materials. In a PL spectroscopy experiment, the excitation energy is usually provided by laser light whose energy is typically larger than the optical band gap. The photoexcited carriers are created, which relax toward their respective band edges or radiative centres and return back to a lower energy level.

For the information, c-Si with the band gap of 1.12 eV at RT is an indirect band gap, which is no PL emission in the visible range at RT. In this work, presence of nanocrystallites embedded within an amorphous matrix in the samples widening the band gap due to QCE and this leads to producing PL emission at a visible range at RT (Ali, 2007; Miura *et al.*, 2006; Shim *et al.*, 2004). In addition, these PL emission characteristics very depending on the size of the Si nanocrystals, with a size of less than 10 nm and its distributions, which control the crystalline volume fraction of the nanocrystals (Ali *et al.*, 2001). Although the quantum confinement of the carriers in Si nanocrystals is the general explanation for the strong PL, there are still some controversial approaches. A model states that PL originates from the localized defects at the Si/SiO_2 interfaces (Ogut *et al.*, 1997; Ledoux *et al.*, 2000; Wang *et al.*, 2008), while the other assigns that the red band is due to quantum confinement supplemented by surface states. The blue band is generally connected to the presence of oxide related defects and the infrared band is related to dangling bonds or band gap luminescence in large crystallites (Fauchet *et al.*, 1996). Thus, the origin of PL from Si nanocrystallites is that both localized defect at the interface and the quantum confinement of excitons is still an important topic in studying the PL characteristics of Si nanostructures.

Figure 3.16 shows the typical PL emission spectrum of nc-Si:H produced by rf PECVD. This spectrum was obtained by using the Micro-Raman/PL spectrometer in Nano-Optoelectronics Research and Technology Laboratory (N.O.R), School of Physics, Universiti Sains Malaysia, which is same spectrometer that was used to obtain the Raman scattering spectra for the same samples. The PL mode is an integrated subsystem that is attached to the system in which the measurement can be performed consecutively, the only difference is changing the laser source for PL measurement.

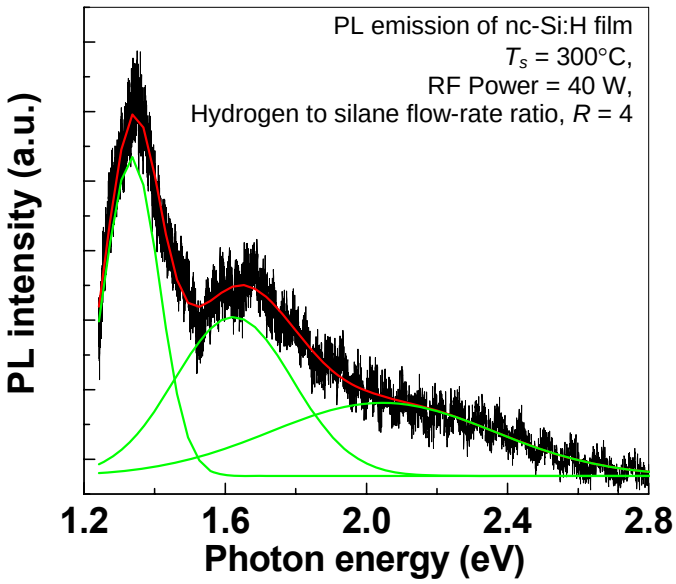

Figure 3.16: A typical PL spectrum of nc-Si:H thin film. The three Gaussian fittings representing the PL emissions from different recombinations (The data is provided from the film deposited at rf power, T_s and R of 40 W, 300°C and 4 respectively).

3.3.6 High Resolution Transmission Electron Microscope (HRTEM)

Transmission electron microscope (TEM) is a challenging technique to study Si nanoclusters in Si nanostructures, mainly in a-Si, SiO_2 and Si_3N_4 matrices (Pavvesi and Turan, 2010). In this system, Si nanoclusters may be either in the amorphous or the crystalline phase. The difficulty lies in separating the host matrix and Si nanoclusters, especially when they are amorphous, since the difference in the atomic number and atomic density does not vary significantly. This results in a low contrast between the Si nanocluster and its matrix in the TEM micrograph. However, the Si nanoclusters in its amorphous matrix can be more secure images by high resolution TEM (HRTEM). This technique works on the principle of coherent superposition of incident and elastically scattered electromagnetic waves from Si nanoclusters. The success of this technique depends on the right orientation of the Si nanoclusters with respect to the incident beam and the thickness of the sample (Mayandi *et al.*, 2007).

Figure 3.17 shows a schematic diagram of a TEM used to study the microstructure of Si:H thin film includes the simplified photon and electron path in (a) an optical and (b) electron microscope, respectively. The electron beams are created by thermoionic effect and accelerated towards the sample by an electric field. Then, the electron beams pass through a condenser lens to obtain parallel beams, then are scanned on a selected area of the sample surface. Simultaneously, the electrons transmitted by the sample are confined and focused by the objective and projector lenses to form the image on the screen. The intensity of the transmitted electron beam determines the brightness of a spot on a screen.

In the transmission electron microscope, the image is formed, magnified, inverted or redressed by means of lenses in a transmission arrangement. The resolution is defined in terms of the minimum distance between two image points that can just be distinguished as two independent points. The minimum distance r can be related to the wavelength λ of the radiation and to the angle α formed by a point object to the objective lens by the relation as (Goodhew *et al.*, 1988),

$$r = \frac{0.61\lambda}{n \sin \alpha}, \tag{3.33}$$

where n is the refractive index of the medium between the object and the objective lens.

In this work, since the concern is the material used, which is mainly biphasic Si:H thin film consisting of nanocrystallites embedded within an amorphous matrix, both absorption and diffraction contrasts are used. The image contrast is due to the variation in intensities of transmitted and diffracted beams depending on the microstructural features and elemental distribution on the electron path in the sample. In imaging mode, when the unscattered beam is the only one admitted through the objective aperture and used for imaging, the atomic number, thickness and density of the target sample determine whether few or many electrons will be transmitted. In an amorphous matrix, any defective part of the material will appear dark on a bright

background and obviously the amount of scattering will determine the contrast (bright field condition). When another diffracted beam is the one selected through the aperture and the central transmitted beam is blocked, the defective part of the specimen will appear bright on a dark background (dark field condition). This will be the case for the nanocrystallites and grains embedded in an amorphous network as well, which allows determining the size of nanocrystals and their orientations by applying the Bragg law in reciprocal space.

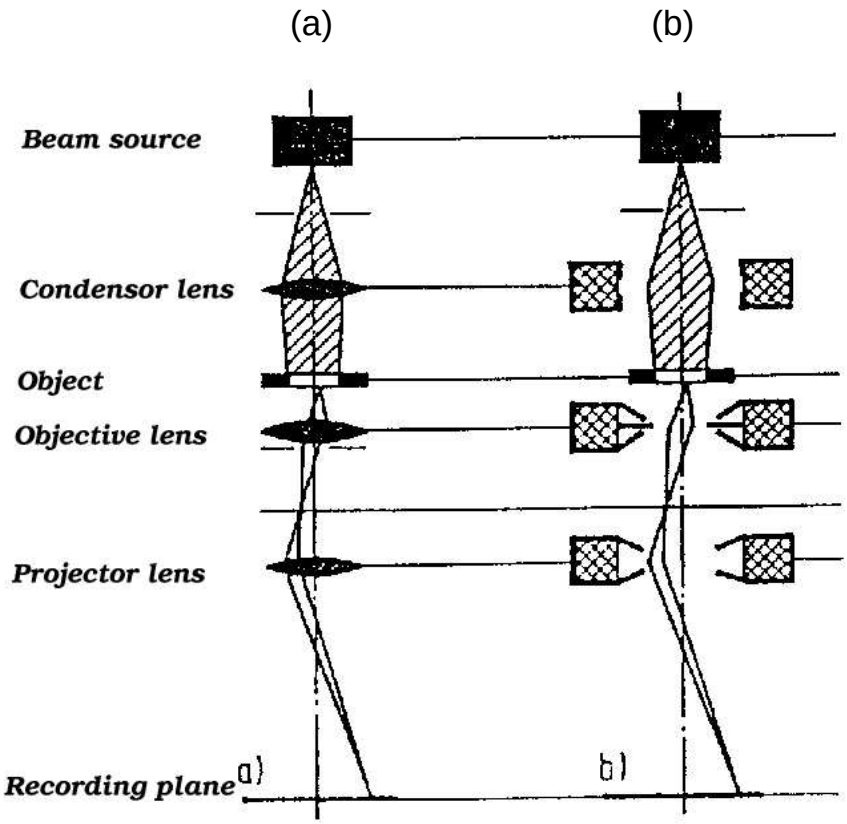

Figure 3.17: A schematic diagram of a TEM includes the simplified photon and electron path in (a) an optical and (b) electron microscope, respectively.

3.3.7 Field Emission Scanning Electron Microscope (FESEM)

Scanning electron microscope (SEM) utilizes an electron beam to produce a magnified image of the sample. In the SEM, an electron beam incident on the sample produces an image while in the field emission SEM the specimen itself is the source of electrons. Commonly, the electron energy is typically 10-30 keV for most samples, but for insulating samples the energy can be as low as several hundred eV. The use of electrons has two main advantages over optical microscopes. Much larger magnifications are possible to achieve by the SEM since electron wavelengths are much smaller than photon wavelengths and the depth of field is much higher. The electron wavelength, λ_e depends on the electron velocity, υ or the accelerating voltage V as (Broglie, 1923),

$$\lambda_e = \frac{h}{m\upsilon} = \frac{h}{\sqrt{2qmV}} = \frac{1.22}{\sqrt{V}}(nm), \tag{3.34}$$

The wavelength is 0.012 nm for V = 10, 000 V which a wavelength significantly below the 400 to 700 nm wavelength range of visible light making the resolution of an SEM much better than that of an optical microscope.

An SEM mainly consists of an electron gun, a lens system, detector and display as shown in Figure 3.18 (Schroder, 1998). Electron emitted from an electron gun pass through a series of lenses to be focused and scanned across the sample. The electron beam should be bright with small energy spread. The most common electron gun is a tungsten filament emitting electrons thermionically with an energy spread of around 2 eV. Tungsten sources have been largely replaced by field emission guns with an energy spread of about 0.2 to 0.3 eV. Field emission guns are about 1000 × brighter than tungsten sources and longer lifetimes. The incident or primary electron beam causes secondary electrons to be emitted from the sample and these are ultimately accelerated to 10 to 12 kV. They are most commonly detected with an Everhart-Thornley (ET)

detector (Everhart and Thornley, 1960). The basic component of this detector is a scintillation material that emits light when struck by energetic electrons accelerated from the sample to the detector. The light from the scintillator is channelled through a lightpipe to a photomultiplier, where the light incident on a photocathode produces electrons that are multiplied, creating the very high grains necessary to drive the CRT. High potentials of 10 to 12 kV are necessary for efficient light emission by the scintillator. So the electron beam will not be influenced by the high ET detector potential, the scintillator is surrounded by a Faraday cage at a few hundred volt potential.

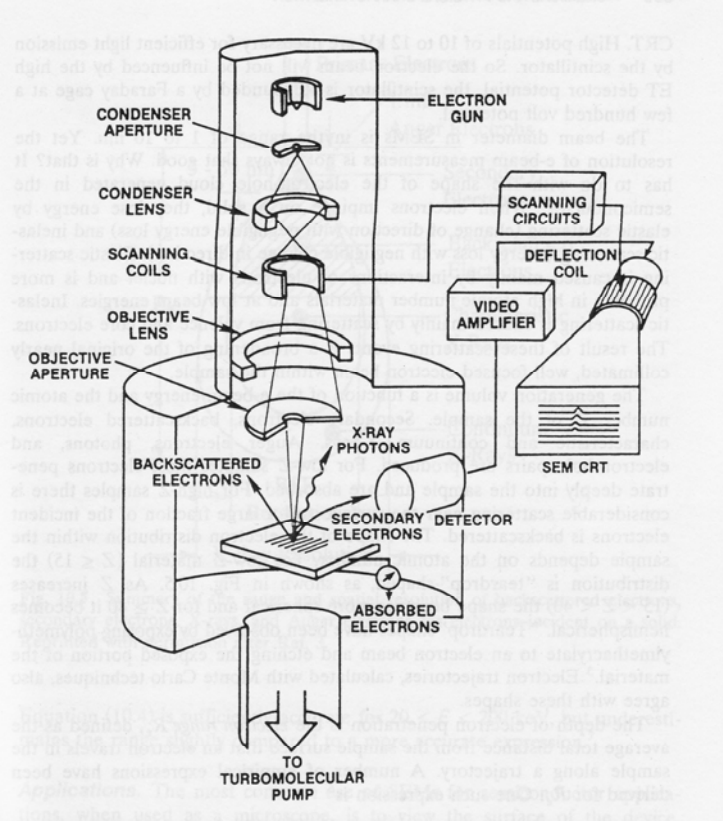

Figure 3.18: A schematic diagram of a SEM (Everhart and Thornley, 1960).